# The Impact of the Inner Angle Steel Tray and Particle Diameter on Dust Removal Efficiency in scrubber tower

Hai Xin[a], Yulin Yan[a], Zhenyu Xu[a], Yong Yang[a], Xianyu Feng[b, *]

[a]*Fushun Mining Group Co., Ltd. shale refinery*

[b]*China National Petroleum Corporation Fushun Petrochemical Branch*

**Corresponding author Email address: 2647136132@qq.com (Xianyu Feng)*

**Funding:** This work was supported by the PhD Start-up Fund (Grant No. 1100130252).

# Abstract

Air pollution, especially particulate pollution, has become a serious issue with the acceleration of industrialization. Wet scrubbers are widely used in industries for air purification due to their advantages. However, most scrubber studies have predominantly focused on fillers and injection methods, neglecting the systematic investigation of the tower rotation angle and particulate physical properties on dust removal performance. In this study, the geometric model of the scrubber was established based on the actual equipment in a refinery. Computational fluid dynamics (CFD) was employed, along with the fluid volume (VOF) and discrete phase (DPM) models, to solve the relevant equations. The grid independence and model were verified. Particles with different diameters were injected into the scrubber with different angle steel tray arrangements (α = 15°, 30°, 45°), and the dust removal efficiency was calculated. The results show that the dust removal efficiency generally increases with the increase of particle diameter. When the particle diameter is 200 - 300μm, the efficiency is consistent. Before 350μm, the highest efficiency is achieved at α = 30°, and the lowest at α = 15°; above 350μm, the highest is at α = 30°, and the lowest at α = 45°. The tray angle affects air distribution uniformity, and α = 45° shows more uniform air distribution. This research provides a scientific basis for optimizing scrubber design and operation. It systematically explores the influence of tray angle and particle diameter on dust removal efficiency, filling the research gap in this area and guiding the improvement of scrubber technology in industrial applications.

**Keywords:** Scrubber; Angle Steel Tray; VOF; DPM; Dust Removal Efficiency

# Article Highlights

1. Found that tray angle and particle size significantly impact dust removal, guiding scrubber design improvements.

2. A 30° tray angle generally yields the highest efficiency for various particle sizes, enhancing air purification.

3. Adjusting tray angle based on particle size can boost performance and reduce energy use in industrial settings.

# 1 Introduction

With the acceleration of industrialization, the problem of air pollution is becoming more and more serious[1], especially particulate pollution, which poses a great threat to human health and ecological environment[2]. Among many air purification technologies, wet scrubber is widely used in chemical, metallurgy, electric power and other industries because of its simple structure, stable operation and easy maintenance, and has become an important means to control particulate matter emissions[3].

The working principle of the scrubber is to make the pollutants in the gas be absorbed or captured by the liquid through the gas-liquid two-phase contact, so as to achieve the purpose of purification[4]. Among them, the relative movement between the air flow in the tower and the spray droplets is very important to improve the efficiency of dust removal[5]. In recent years, with the development of computational fluid dynamics (CFD) technology, numerical simulation[6] has become an effective tool for studying the internal flow characteristics of scrubbers and optimizing their structural design[4]. The precise mathematical model is established to simulate the flow field distribution, interphase mass transfer process and particle trapping mechanism in the tower under different working conditions[7]. Researchers [8] managed to understand the crucial factors influencing the dust - removal efficiency of scrubbers. This understanding offers theoretical guidance and technical support for practical engineering applications. It helps engineers design and operate scrubbers more effectively, enabling them to optimize the scrubber's performance, such as enhancing dust - removal efficiency and reducing energy consumption. By identifying these key factors, the research paves the way for better - informed decisions in the development and improvement of scrubber systems used in various industrial processes.

Xu et al.[9] conducted a study on the formation of particulate matter during the incineration of municipal solid waste and the emission outcomes after treatment with a semi - dry flue gas deacidification scrubber. They employed a systematic on - site measurement approach. The findings of their research indicate that the particle size distribution exhibits a three - peak pattern. Among these, particles in the size range of 0.3 - 3μm account for the largest proportion. This information is valuable as it provides insights into the characteristics of particulate matter in this specific context, which can help in understanding the performance of the scrubber and the effectiveness of waste treatment processes. Zhu et al.[10] used CFD simulation technology to study the diffusion characteristics and influencing factors of particulate matter in ship exhaust plume under Arctic environment. It is found that the yaw Angle has the greatest effect on the dispersion of particulate matter. Tao et al.[11] studied the multi-scale dynamic distribution characteristics of dust particles in wet precipitators by using multi-scale analysis method based on image field. It is found that the grayscale signal of dust particles in gas-liquid two-phase flow has obvious fractal characteristics, and different scale subsets reflect the dynamic distribution characteristics of dust particles at individual, aggregate and macroscopic levels. Copeland[12] constructed a novel dust tower to evaluate the effect of different dust inhibitors on iron ore pellets by directly measuring the amount of dust raised by the material. Kim et al.[13] studied the effect of electric spray system (EFI) on the removal efficiency of fine particles by introducing it into the spray tower. The results show that a large number of small droplets generated by the EFI system increase the electrostatic attraction and collision frequency between the droplets and the particles, thus improving the removal efficiency of the particles. Bacher and Riebel[14] experimentally investigated the role of electrohydrodynamic (EHD) effects in enhancing mass transfer by combining a wet pilaster with an electrostatic precipitator. It was found that the EHD effect can significantly increase the mass transfer coefficient, with the enhancement factor varying between 3-8, depending on the operating conditions and discharge electrode design. Sen et al.[15] uses CFD to study the effect of different sieve plate arrangements (such as cross-flow, counterflow, etc.) and he relative positions of internal components (such as gas distributors, downcomers, etc.) on specific interface areas. Amitava[16] studied the $SO_2$ washing performance of a conical bubble tower with internal components on particle loads, and established an empirical correlation formula for predicting the removal efficiency. The predicted values fit well with the experimental values. Ji et al.[17] studied the influence of inner components of bubble tower with low aspect ratio through experiments and simulations. After model verification, it was found that the number of components had little effect on gas holdup but changed its radial distribution, affecting liquid velocity, flow pattern and turbulence characteristics.

However, most previous studies have predominantly concentrated on the impact of particle signal analysis and the addition of an electric spray system on the dust - removal performance. Moreover, although the physical properties of particulate matter, such as particle size and density, have a substantial effect on the dust - removal capabilities of scrubbers, there has been a lack of comprehensive and systematic research in this area.

Consequently, this paper undertakes an investigation into the influence of the tower rotation angle and particle diameter on the scrubber's dust - removal efficiency. It employs experimental and numerical simulation methods to achieve this. The ultimate goal is to offer a scientific foundation for optimizing the design of scrubbers and enhancing their environmental protection efficiency. This research fills a crucial gap in the existing knowledge and can contribute to more effective air - purification solutions in industrial applications.

The primary goal of this paper is to construct a three - dimensional numerical model. This model was designed to simulate the gas - liquid two - phase flow within the scrubber, taking into account complex phenomena like bubble breakage and coalescence (Sec. 2). In Sec.3, we comprehensively analyzes the flow characteristics, volumetric concentrations, mixing behavior, and dynamic fields for different tray alignments. Additionally, it proposes the underlying physical mechanisms. Finally, summary and discussion are given in Sec. 4.

# 2 Methodology

## 2.1 Geometric model of scrubber

Fig.1 is a photo of the washing and saturation tower in the refinery. The upper part is the scrubber section and the lower part is the saturation section. After the oil shale is pyrolytic, the pyrolysis gas produced will contain a certain amount of solid impurities, which will be introduced into the scrubber through the pipeline for treatment. First, it will enter the double-row finned gas distributor in the scrubber, then pass through the 4-layer angle steel tray, and continue to pass through the trough liquid distributor. The reverse contact between the washing liquid and the gas will always occur in the whole process. The addition of some internal components for increasing the degree of turbulence in the tower is mainly used to increase the contact degree of gas and liquid, and improve the cooling and dust removal efficiency of dust gas.

Fig.1a shows the washing saturation tower. The washing tower is used to purify and cool the dust-containing gas, and the saturation tower is used to produce saturated steam. The water seal groove in the middle of the two towers, which is designed to prevent gas leakage between the two sections and maintain the pressure balance, cannot be clearly displayed. Fig.1b shows the fluted liquid distributor for increasing the turbulence degree of the fluid. After entering the scrubber through the pipeline, the washing liquid is first spread on the primary groove of the fluted liquid distributor, in which there are two primary grooves and several holes are cut at the lower part of the primary groove for the fluid to lead to the secondary groove. Each two are connected in series, which is conducive to the uniform distribution of fluid. The secondary slots are dispersed to the same horizontal plane in parallel and evenly according to the diameter of the scrubber. The lower part of each secondary slot is also opened with several small holes for the fluid to spray evenly into the tower. The feature of this device is that no external power is required, and the fluid can be evenly dispersed into the tower under the action of gravity. And the trough liquid distributor has a certain gap between each groove to ensure the permeability of the fluid. After falling, the washing liquid will pass through Fig.1c, which is the angle steel tray, which is also the object studied in this paper. Fig.1d is a simple diagram of the inside of the scrubber, which is convenient for understanding the internal structure of the actual photo. There are four layers of angle steel tray in the scrubber, and the length of angle steel tray varies with the type according to the different diameter of the tower. However, each two adjacent layers will have a certain dislocation angle (a certain rotation angle from the top down), this paper mainly studies the rotation angle α=15°, α=30° and α=45°, In the study of Zhao et al.[18], since the shape of the tray is both axisy-symmetric and centrosymmetric, it will coincide with the original position every 90° rotation, so combined with the actual operation of the equipment, the three dislocation angles studied are selected to ensure full contact between gas and liquid. A double-row finned gas distributor is also designed at the entrance of the dust-containing gas inside the scrubber, which is used to increase the turbulence degree of the gas, so that the gas is evenly dispersed into the tower, and prevent the local concentration of the gas from being high or low, which affects the dust removal efficiency. The arrangement in the saturation tower is the same as that in the scrubber but the flow medium inside is different.

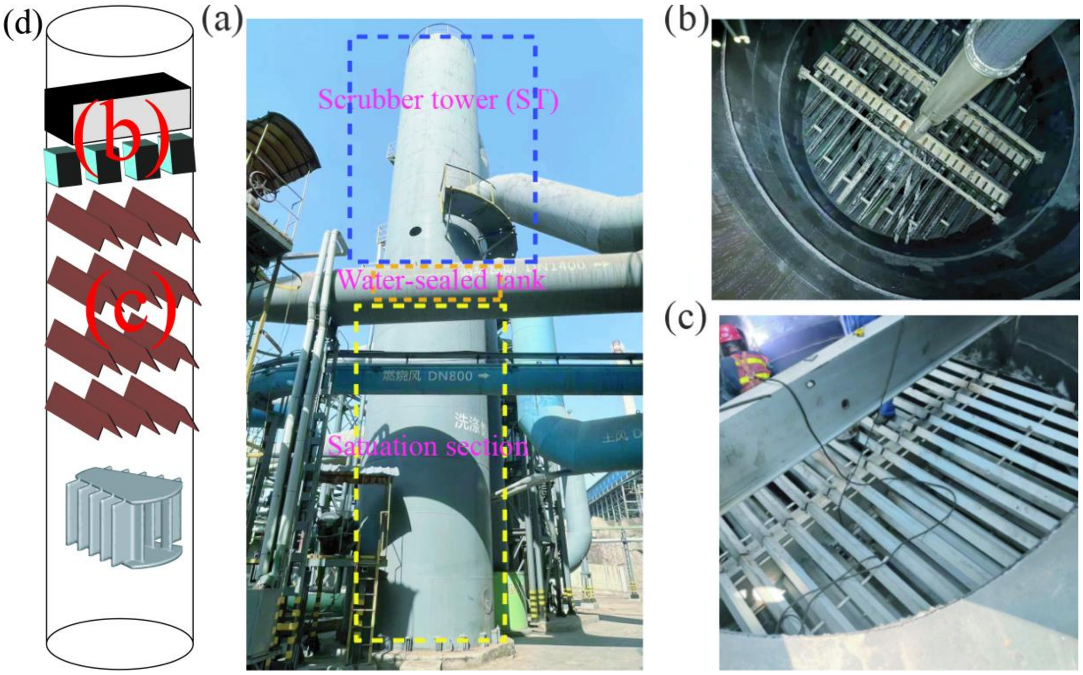


**Fig.1 Washing saturation tower of the Shale Oil Refinery factory: (a) Washing saturation tower; (b) slot-type liquid distributor; (c) a layer of strip-type tray; (d) Simple diagram of the inner structure of the tower.**

The total height of the washing and saturation tower, which includes both the scrubber section and the saturation section, is not explicitly provided in Fig. 1 but is an important overall dimension. In the study, the relevant height parameter for the scrubber section is further detailed in the text as H1 = 14100mm (as shown in Table 1). This height determines the overall space available for gas-liquid-solid interactions and affects the residence time of the gas and particles within the scrubber. The inlet diameter of the gas is Φ3 = 1600mm, which determines the amount of gas that can enter the system. The distance from the gas distributor to the bottom tray is H3 = 1680mm (excluding the thicknesses of the gas distributor and tray).

The angle steel trays are arranged in four layers with a certain dislocation angle (α = 15°, 30°, or 45°). The distance between each adjacent layer is H4 = 1000mm (excluding the thicknesses of the trays). This distance affects the gas-liquid-solid mixing and the opportunity for particles to interact with the trays and liquid at different levels within the scrubber.

The fluid distributor is located at the top of the washer and is connected to the water inlet pipe, it plays a crucial role in distributing the washing liquid evenly across the cross-section of the tower. The inlet diameter of the scrubber water is Φ2 = 250mm, which affects the flow rate and pressure of the incoming liquid. The liquid distributor has a certain design with primary and secondary grooves and small holes for fluid dispersion. The vertical distance from the liquid distributor to the upper tray is H5 = 1000mm (excluding the thicknesses of the liquid distributor and tray). This distance influences the initial distribution of the liquid and its interaction with the gas and particles as they flow downwards through the scrubber.

Given our intention to explore the flow distribution and dust removal of dust - laden gas within the tower, through an analysis of the actual operation of the washing saturation tower, it is evident that the dust - laden gas solely flows through the scrubber. Consequently, the scope of this study encompasses the scrubber section and the water seal tank at the lower part. Notably, the four - layer angle steel tray provides the largest contact area between the gas and the washing liquid. This area is crucial as it significantly influences the efficiency of the dust - removal process. A larger contact area allows for more opportunities for the gas - liquid interaction, facilitating the capture of dust particles by the washing liquid. This, in turn, can improve the overall performance of the scrubber in removing dust from the gas stream.

In the present study, the types and arrangements of the tray are various, and the same time, multiple layers of the tray are arranged inside the tower to increase the contact area. The angle steel tray used in this study is center symmetric, that is, it will overlap with the original figure after rotation of 180°. Therefore, in order to maximize the possibility of falling washing liquid always falling on the tray, which can not only increase the surface area of the washing liquid, but also continuously wash the tray to improve the dust removal efficiency of the dust-containing gas, it is also necessary to consider the dislocation angle of the tray.

The tray of the scrubber studied by Tseng and Li[19] et al. is shaped like a sieve plate, that is, the tray arranged in the scrubber is disc-shaped, and several holes are cut in the disc to change the gas-liquid contact by changing the specific surface area of the porosity. Abbasnia[20] et al. also studied sieve tray. The control of the specific surface area of the porosity of this tray requires certain technologies. If the porosity is too small, the airflow will be blocked, and if it is too large, the washing effect will be affected. Compared with the angle steel tray with the dislocation arrangement between different layers, the design and manufacturing process of the angle steel tray is simpler and more convenient, but it can increase the gas-liquid contact more effectively. Due to the large spacing between each angle steel, it can effectively prevent dust blockage inside the scrubber. The angle steel material can be carbon steel or stainless steel and can be corrosion-resistant. The same washing performance can be achieved compared to more complex tray designs.

## 2.2 Computational domain

Fig.2 shows the geometric model of the scrubber in Cartesian coordinate system using 3D mapping software[18]. Fig. 2a presents the size diagram of the scrubber, enabling a direct visualization of the dimensions of each component within the scrubber. This diagram serves as a crucial reference for understanding the spatial configuration of the scrubber, which is essential for analyzing the flow dynamics and performance of the system. Fig. 2b depicts the trough liquid distributor, positioned at the top of the scrubber and connected to the water inlet pipe. Its function is to enhance the transverse diffusion of the washing liquid, ensuring a more uniform distribution of the liquid across the cross - section of the scrubber. This uniform distribution is vital for maximizing the contact area between the washing liquid and the dust - laden gas, thereby improving the dust -

removal efficiency. Fig. 2c shows the double - row finned gas distributor, located at the inlet of the dust - containing gas within the scrubber, specifically at the innermost part and on the upper side of the tower bottom. This distributor plays a significant role in promoting the transverse diffusion of the inlet gas. By increasing the gas's transverse diffusion, it helps to evenly disperse the gas in the scrubber, facilitating better mixing with the washing liquid and enhancing the overall performance of the scrubber. Fig. 2d - f illustrate the angle steel tray, an internal component under study. Positioned between the trough liquid distributor and the double - row finned gas distributor, the angle steel tray is crucial for the gas - liquid - solid interactions in the scrubber. The tray's design and arrangement influence the flow path of the gas, liquid, and particles, ultimately affecting the dust - removal efficiency. In Fig. 2 (g), which represents the cross - section of the angle steel tray, the angle steels are spaced at regular intervals, with a designed distance of 10 cm between adjacent angle steels. This distance is a critical parameter. An excessively large separation between the angle steels can lead to insufficient gas - liquid contact, reducing the effectiveness of the scrubber in removing dust particles. Conversely, an excessively small distance can increase the flow resistance of the fluid within the system, consuming more energy and potentially affecting the overall flow dynamics. The angle steel tray consists of four parallel and misaligned layers. The consistent distance between adjacent layers and the identical dislocation angle contribute to the tray's unique flow - guiding properties. The misalignment of the layers helps to create a tortuous flow path, enhancing the mixing of the gas, liquid, and particles and increasing the chances of dust particle capture. In the operation process of the scrubber, water needs to be supplied by the external water pump, the flow rate of the washing pump is 486$m^3$/h, and the head is 38.5m. The researched scrubber equipment parameters are Φ4200mm ×14100mm, the inlet diameter of the scrubber water is Φ1 250mm, the outlet diameter is Φ4 450mm, the inlet diameter of the gas is Φ3 1600mm, and the outlet diameter is Φ4 1600mm.

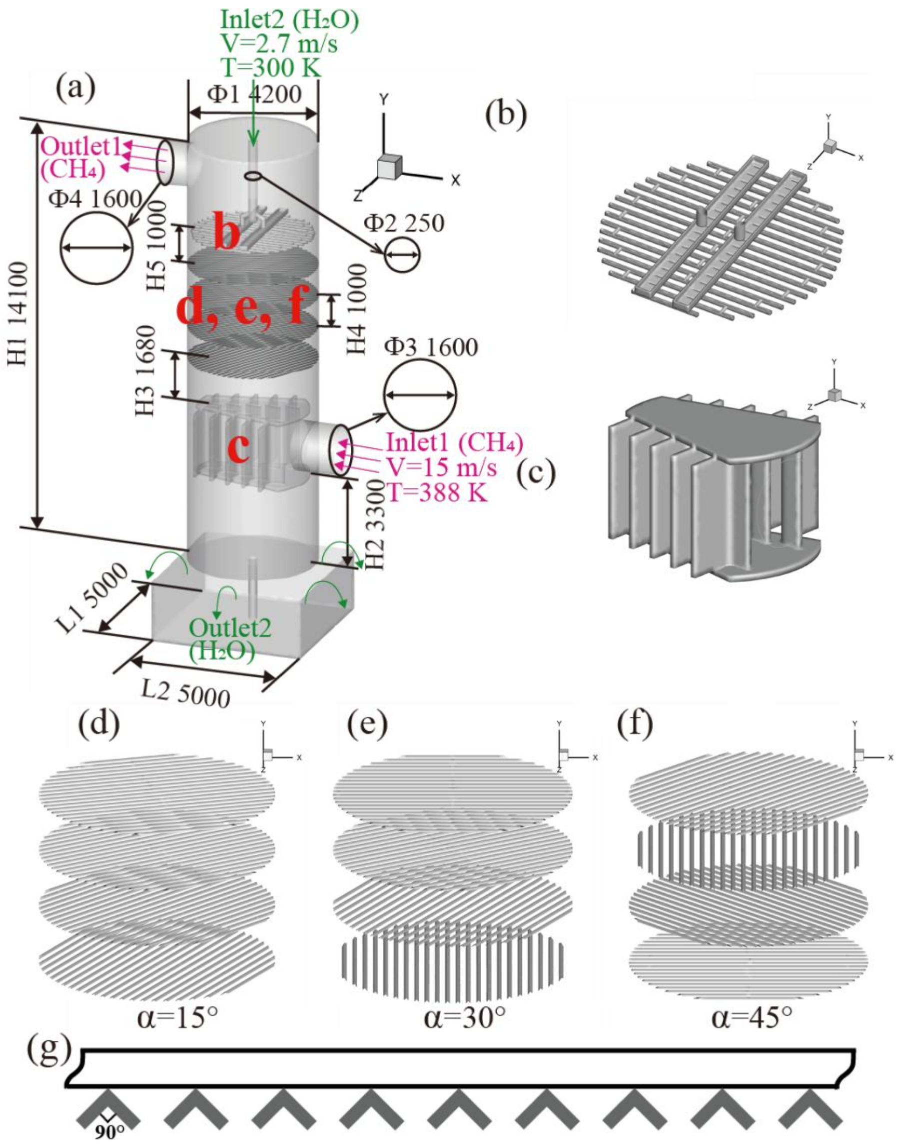


**Fig.2 Geometry model of the scrubber and internal components: (a) The scrubber and its dimensions (unit: mm, see Tab.1); (b) liquid distributor (for $H_2O$); (c) fin-type gas distributor (for $CH_4$); (d) α=15°; (e) α=30°; (f) α=45°; (g) cross section of a tray .**

In order to more easily and intuitively see the detailed dimensions when drawing the geometric model, the symbols, dimensions and descriptions used in drawing the scrubber model are listed in Tab.1.

**Tab.1 Summary of the key spatial dimensions of the geometry model annotated in Fig.3**

| Symbols and dimensions (mm) | description | Symbols and dimensions (mm) | description |
|---|---|---|---|
| Φ1 (4200) | diameter | H1 (14100) | Scrubber height |
| Φ2 (250) | Water inlet | H2 (3300) | Vertical distance |

| | | | |
|---|---|---|---|
| | diameter | | from the air intake to the bottom of the scrubber (excluding the thickness of the air intake component) |
| Φ3 (1600) | Air intake diameter | H3 (1680) | Vertical distance from the gas distributor to the bottom tray (excluding the thicknesses of the gas distributor and tray) |
| Φ4 (1600) | Air outlet diameter | H4 (1000) | Vertical distance between adjacent trays (excluding the thicknesses of the trays) |
| L1*L2 (5000*5000) | Water seal groove length x width | H5 (1000) | Vertical distance from the liquid distributor to the upper tray (excluding the thicknesses of the liquid distributor and tray) |

Angle steel trays are made of corrosion-resistant carbon or stainless steel[21]. The zigzag structure formed by multiple parallel angles enhances the development of turbulence[22]. Three different tray arrangements are considered here: α=15, α=30, and α=45, where α represents the misalignment between two adjacent parallel tray layers in each tray arrangement scheme. The dislocation effectively changes the shape formed by the tray inside the scrubber, thus changing the flow path of the flow field, thus affecting the direct washing of the gas phase. Through simulation to determine an optimal α can achieve gas purification performance. Adequate mixing in both horizontal and vertical directions facilitates particle capture.

## 2.3 Mathematical model

In the simulation process, the governing equations need to be solved when calculating the fluid. Assuming that the material used is an incompressible fluid, the mass, momentum and energy equations need to be solved:

Mass equation[23]:

$$\frac{\partial(\rho u)}{\partial x}+\frac{\partial(\rho v)}{\partial y}+\frac{\partial(\rho w)}{\partial z}=0 \qquad (1)$$

$\rho$ represents the fluid density, and $u$, $v$, and $w$ are the velocity components of the fluid in the $x$, $y$, and $z$ directions, respectively. Equation (1) describes that the sum of the mass fluxes of the fluid in the three directions is zero, ensuring the conservation of the mass of the fluid in a given space. In a scrubber, the equation is helpful to understand the mass distribution of gas and liquid at different positions.

Momentum equation[24]:

$$\rho u\frac{\partial u}{\partial x}+\rho v\frac{\partial u}{\partial y}+\rho w\frac{\partial u}{\partial z}=-\frac{\partial p}{\partial x}+\mu\left(\frac{\partial^2 u}{\partial x^2}+\frac{\partial^2 u}{\partial y^2}+\frac{\partial^2 u}{\partial z^2}\right)+\rho g_x \qquad (2)$$

$$\rho u\frac{\partial v}{\partial x}+\rho v\frac{\partial v}{\partial y}+\rho w\frac{\partial v}{\partial z}=-\frac{\partial p}{\partial y}+\mu\left(\frac{\partial^2 v}{\partial x^2}+\frac{\partial^2 v}{\partial y^2}+\frac{\partial^2 v}{\partial z^2}\right)+\rho g_y \qquad (3)$$

$$\rho u\frac{\partial w}{\partial x}+\rho v\frac{\partial w}{\partial y}+\rho w\frac{\partial w}{\partial z}=-\frac{\partial p}{\partial z}+\mu\left(\frac{\partial^2 w}{\partial x^2}+\frac{\partial^2 w}{\partial y^2}+\frac{\partial^2 w}{\partial z^2}\right)+\rho g_z \qquad (4)$$

$p$ is the fluid pressure, $\mu$ is the fluid viscosity, and $g_x$, $g_y$, and $g_z$ are the components of gravity in the $x$, $y$, and $z$ directions, respectively. These equations describe how the fluid velocity changes in three directions due to factors such as pressure differences, viscosity, and gravity. The pressure gradients ($\frac{\partial p}{\partial x}$, $\frac{\partial p}{\partial y}$, $\frac{\partial p}{\partial z}$) cause the fluid to flow, while the viscosity of the fluid (the $\mu$-dependent term) hinders this flow. In the scrubber, it is possible to calculate how gases and liquids flow around the tray and other components.

Energy equation[25]:

$$\rho C_p u \frac{\partial T}{\partial x} + \rho C_p v \frac{\partial T}{\partial y} + \rho C_p w \frac{\partial T}{\partial z} = k\left(\frac{\partial^2 T}{\partial x^2} + \frac{\partial^2 T}{\partial y^2} + \frac{\partial^2 T}{\partial z^2}\right) + S_T \qquad (5)$$

$C_p$ is the specific heat capacity of the fluid at constant pressure, $T$ is the temperature of the fluid, $k$ is the thermal conductivity of the fluid, and $S_T$ is the heat source term. This equation describes the transfer and transformation of energy within a fluid, taking into account the effect of heat conduction (expressed by thermal conductivity $k$) and other energy sources or sinks ($S_T$) on the fluid energy. In research, this equation helps to understand the temperature changes of gases and liquids when they interact with each other and with particles, which is critical for processes such as heat transfer and evaporation.

Turbulent kinetic energy equation[26]:

$$\frac{\partial \rho k u_i}{x_i} = \frac{\partial}{\partial x_j}\left(\mu \frac{\partial k}{\partial x_j}\right) + G_K + G_b - \rho\varepsilon \qquad (6)$$

$$\frac{\partial \rho \varepsilon u_i}{x_i} = \frac{\partial}{\partial x_j}\left(\mu \frac{\partial \varepsilon}{\partial x_j}\right) + C_{1\varepsilon}\frac{\varepsilon}{k}(G_k + G_{3\varepsilon}G_b) - \frac{\rho\varepsilon^2}{k} \qquad (7)$$

where $k$ is the turbulent energy in $m^2/s^2$ , $\varepsilon$ is the turbulent dissipation rate in $m^2/s^3$ , $G_k$ is the generation of turbulent kinetic energy that arises due to mean velocity gradient, $G_b$ is the generation of turbulent kinetic energy that arises due to buoyancy. $C_{1\varepsilon}$ , $C_{2\varepsilon}$ , $C_{3\varepsilon}$ , and $C_\mu$ are empirical constants and their values are 1.44, 1.92, 0.0, and 0.09, respectively.

Equation (6) describes the distribution of turbulent kinetic energy in space. In scrubbers, turbulence helps to mix gas-liquid two phases more effectively, enhance the contact between particles and droplets, and improve the chance of particle capture. Therefore, understanding and predicting turbulence characteristics is crucial for optimizing scrubber performance. Equation (7) describes the spatial distribution of turbulent kinetic energy dissipation, which is related to equation (6). By solving these two equations simultaneously, we can better understand the turbulent characteristics of the flow in the scrubber and its influence on the overall performance.

Particle motion trajectory equation[24]:

$$m_p a_p = F_D + F_G + F_a \qquad (8)$$

$m_p$ is the particle mass, $A_p$ is the particle acceleration, $F_D$ is the drag force, $F_G$

is the gravity force. The equation describes the law of acceleration of particles under the action of various forces, and determines the acceleration of particles at a certain position through the balance relationship of forces, thus affecting their motion trajectory.

$$F_D = \frac{1}{2}\rho C_D A_p \left(v - v_p\right)\left|v - v_p\right| \quad (9)$$

$\rho$ is the fluid density, $C_D$ is the drag coefficient, $A_p$ is the cross-sectional area of the particles, $v$ is the fluid velocity, and $v_p$ is the particle velocity. This equation calculates the force exerted by the fluid as the particle moves through the fluid. The drag force depends on the fluid density $\rho$, the drag coefficient $C_D$, the cross-sectional area $A_p$ of the particle, and the relative velocity $v - v_p$ between the fluid and the particle. The drag force impedes the motion of particles and is the key factor that determines the motion state of particles in fluid.

$$F_G = m_p g \quad (10)$$

$m_p$ is the particle mass and $g$ is the acceleration of gravity. This equation calculates the force of gravity on the particle, the magnitude of which is proportional to the particle mass $m_p$ and the acceleration of gravity $g$, and the gravity always acts on the particle to make it move downward.

$$C_D = a_1 + \frac{a_2}{\mathrm{Re}} + \frac{a_3}{\mathrm{Re}^2} \quad (11)$$

$\mathrm{Re}$ is the Reynolds number, and $a_1$, $a_2$, and $a_3$ are empirical constants. This equation is used to calculate the drag coefficient, which depends on the Reynolds number $\mathrm{Re}$, a dimensionless quantity used to characterize the flow state around the particles. The empirical constants $a_1$, $a_2$, and $a_3$ are used to fit the equation to the experimental data in order to accurately calculate the drag coefficient under different flow conditions. By understanding these forces and their effects on particle motion, it is possible to predict the trajectory of particles within the scrubber and their likelihood of being captured by liquids or other components.

## 2.4 Boundary conditions and calculation methods

When operating a scrubber, the initial step is to conduct a flow field simulation. This simulation is run until the flow field reaches a stable state. Once stable, particles are introduced to assess the dust removal efficiency. The scrubber model used in this study is based on the actual factory - scale design. As such, the boundary conditions applied in the simulation are representative of those during real - world operation. This approach ensures that the simulation results closely approximate the actual performance of the scrubber in an industrial setting, providing valuable insights into its dust - removal capabilities under practical conditions. Inlet 1 is the inlet of the dust-containing gas, and the inlet speed and temperature are 15m/s and 388K, respectively. Inlet 2 is the inlet of washing liquid, and the inlet speed and temperature are 2.7m/s and 300K, respectively. The outlet adopts the pressure outlet boundary condition and the pressure is set to zero. No slip boundary condition is assumed on an adiabatic solid surface.

After completing the flow field calculation, the DPM is selected for further analysis. DPM is chosen because it can precisely represent the interaction between the fluid and the particles. Given that the particles carried by the gas typically have small diameters, particle - particle collisions are not taken into account in this study. In the calculation process, the continuous phase and discrete phase are computed under distribution control. Specifically, once the flow field has completed 10 iterations, a particle is injected, and then the iteration is finalized, after which the detailed information of the particle is calculated. To accurately track the particle trajectory, the number of particle - tracking steps is set as large as possible. In this research, the number of steps is set to 50,000 to ensure that each particle's movement can be effectively captured. Moreover, several forces are considered in the model. These include the thermophore force, Saffman lift force, virtual mass force, and pressure gradient force. Additionally, the drag force is described using the spherical criterion. This comprehensive approach allows for a more accurate simulation of the particle behavior within the scrubber system, contributing to a better understanding of the dust - removal process.

The injection surface was selected as the gas inlet plane, the type of injection particles was inert particles, and the particle material was selected as anthracite pulverized coal particles in the system, with particle density of 2000 kg/m$^3$, specific heat capacity of 1650 J/(kg·K), and thermal conductivity of 0.35 W/(m·K). The setting of particle diameter is similar to the research method of Sun et al[27]. The particle diameter is selected as rosin-rammler (R-R) distribution, the diameter range is 10-3000 μm, and the number of diameter is set as 10. The default dispersion coefficient is 3.5.

The initial velocity is the same as the initial velocity of the gas phase inlet, and the gas inlet surface is sprayed in the normal direction, and the velocity is 15m/s. In the discrete phase simulation, the dust removal efficiency is discussed by capturing the particles. In this paper, when the particle flow rate is constant, five groups of particle jets are set up in five times, and the average particle size is 100μm, 200μm, 300μm, 400μm, 500μm, respectively. The inlet mass flow rate of particles is constant at 1e$^{-20}$kg/s. The inlet and outlet boundary conditions are set as escape, that is, particles are allowed to enter and exit. For the trough liquid distributor, angle steel tray, water seal tank wall and the lower bottom surface of the scrubber, the trap of particles is set. The boundary conditions for the rest of the walls are set as elastic impact reflection. There is no need to initialize again during calculation, and particles need to be added and calculated on the basis of the previously calculated flow field. Tab.2 summarizes the physical properties of air, $CH_4$, $H_2O$, and particles, including density, thermal conductivity, specific heat capacity, and viscosity.

**Tab.2 Physical parameters for the air, $CH_4$, $H_2O$ and Particle**

| Parameter | Air | $CH_4$ | $H_2O$ | Particle | Unit |
|---|---|---|---|---|---|
| Density | 1.225 | 0.6679 | 998 | 2000 | kg m$^{-3}$ |
| Dynamic viscosity | $1.7894\times10^{-5}$ | $1.087\times10^{-5}$ | 1000 | -- | kg m$^{-1}$ s$^{-1}$ |
| Heat conductivity | 0.0242 | 0.0332 | 0.6 | 0.35 | W m$^{-1}$ K$^{-1}$ |
| Capacity | 1006.43 | Calculated | 4182 | 1650 | J kg$^{-1}$ m$^{-3}$ |

In this paper, the pressure-velocity coupling method is used to solve the control equation, and the pressure term is PRESTO! calculate. Standard atmospheric pressure is used as reference pressure in calculation.

The integration time step of the pseudo-transient method is 0.01s, which satisfies the Courant-Friedrich-Lewy condition. Although the pseudo-transient method is not a true transient, it is essentially an implicit underrelaxation scheme, and the introduction of the concept of time steps enhances the convergence to the final steady-state result. The initial inlet is a fluid inlet, and the water phase of the liquid region in the water seal tank is 1, that is, the tank is full of water. The iterative calculation starts after the end of the initialization, and the calculation stops when all physical quantities reach a stable value.

## 2.5 Grid independence verification and model verification

Fig.3 shows the grid division of scrubber calculation domain, which adopts unstructured grid. Fig.3b-e shows the mesh refinement of the inner components of the scrubber, so that the flow of fluid and particles can be calculated more accurately and the calculation accuracy can be improved.

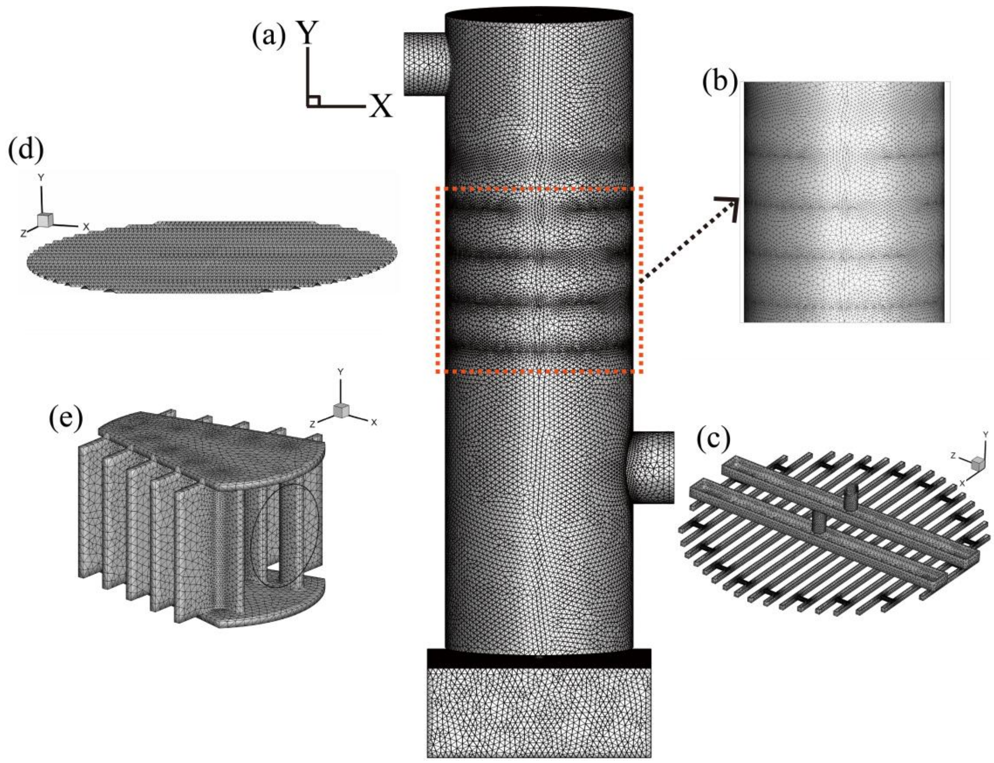


**Fig.3 Grid division of scrubbers and grid refinement diagram of internal components**

In order to ensure that the number of grids divided can reach the accuracy required by the calculation, it is necessary to verify the grid independence of the calculation domain first. This study was divided into 6 groups of grids, with the number of grids being 1.6 million, 2.1 million, 2.6 million, 3 million, 3.5 million and 4 million, respectively. Each grid was calculated according to the same calculation setting and calculation method, and the convergence between the average velocity value of the Outlet 1 plane and the temperature of the monitoring point (-2.5. 8, 0.05) in the center of the Outlet 1 plane was detected. The calculation results are drawn in Fig.4.

As shown in Fig.4, we compared the results of different grid numbers in terms of temperature and velocity changes at the monitoring point. While a higher grid number generally leads to more accurate results, it also requires significantly more computational resources and time. When dividing the grid, the calculation method of capturing the slit and curvature is adopted, which can divide a finer grid in the sharp or complex parts of the model, and can calculate the fluid movement near the complex area more accurately. Therefore, a lot of time and memory are consumed during CFD calculation. As can be seen from Tab.3, compared with the 3.5 million grid model, the calculation time of the 4 million grid model is much longer, and the accuracy is only slightly improved. On the other hand, compared with the 3.5 million grid model, the 3 million grid model has larger deviations in temperature and velocity. After careful consideration of these trade-offs, we determined that the 3.5 million grid configuration strikes a good balance between computational efficiency and accuracy. It provides results that are sufficiently accurate for our study while keeping the computational cost within a reasonable range.

Considering the calculation accuracy and computing resources comprehensively, the calculation model is more suitable for 3.5 million grids, where the temperature changes within 5% and the speed changes within 8%. Therefore, the accurate calculation of 3.5 million grids is followed to ensure that the relative error between the simulation results and the actual values running in the plant is minimized.

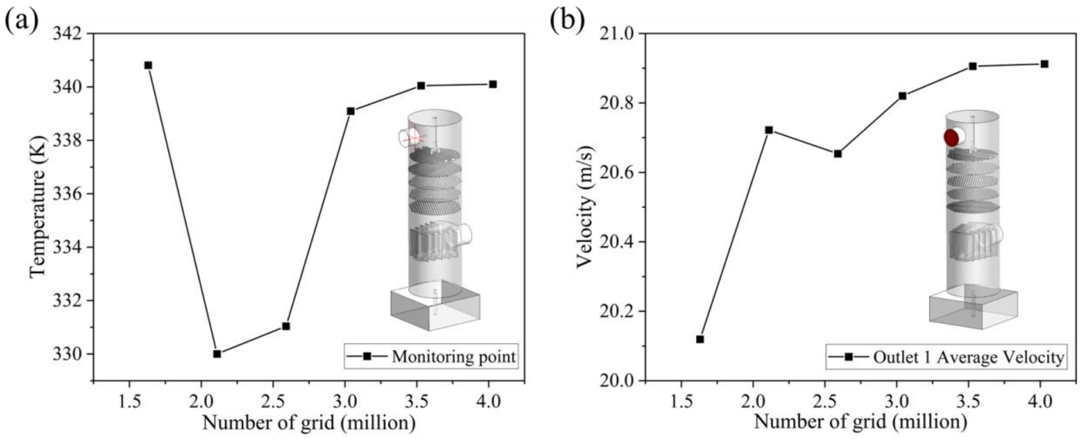


**Fig.4 Grid independence test. Variations of (a) temperature, and (b) velocity at the monitoring point located at the center of Outlet1**

After the 3.5 million grid calculation is completed, the simulation results are compared with the factory measurement data in Tab.3. For the monitored data and measured factory values are in good agreement, Outlet1's exit speed simulation value is slightly larger than the measured value, but the relative error is 8%, which meets the calculation standard. The temperature monitoring values of Outlet 1 and Outlet 2 are slightly lower than the measured values, which is caused by the fact that the tower wall is regarded as adiabatic in the simulation calculation and the heat loss is ignored. The corresponding relative errors are 4.84% and 5.65% respectively, which are both less than 10% and meet the calculation standards.

**Tab.3 Quantitative comparison of simulation results against the measured data at the factory**

| Project | Outlet1 T (K) | Outlet1 V (m/s) | Outlet2 T (K) |
|---|---|---|---|
| Measured value | 348.5 | 19.3 | 347.9 |
| RANS solve | 331.6453 | 20.84412 | 328.23 |
| Relative error | 4.84% | 8% | 5.65% |

The behavior of the near wall between the wall and the first layer grid is based on the research of Kalitzin et al[28] in the parameterization of the wall law. The maximum $Y^+$ is maintained in the range of 30-300, ensuring the accuracy of fluid flow in the grid cells adjacent to the wall, which can be corrected by the corresponding wall function.

Due to the inaccessibility of internal measurements within the company's scrubber tower, a point-by-point comparison of the 3D field inside the tower cannot be conducted. However, using the RANS and $k-\varepsilon$ turbulence models, the performance of the model in mixing two fluids in a T-junction flow field was further evaluated with respect to the experiment of Lin et al[29]. As shown in Fig.5, the predicted temperature distributions along the monitoring points T1 - T3 - T5 agree well with the relevant measured values within the error bars. Although there are some larger discrepancies along T2 - T4 - T6, the model effectively captures the general pattern of the temperature distribution.

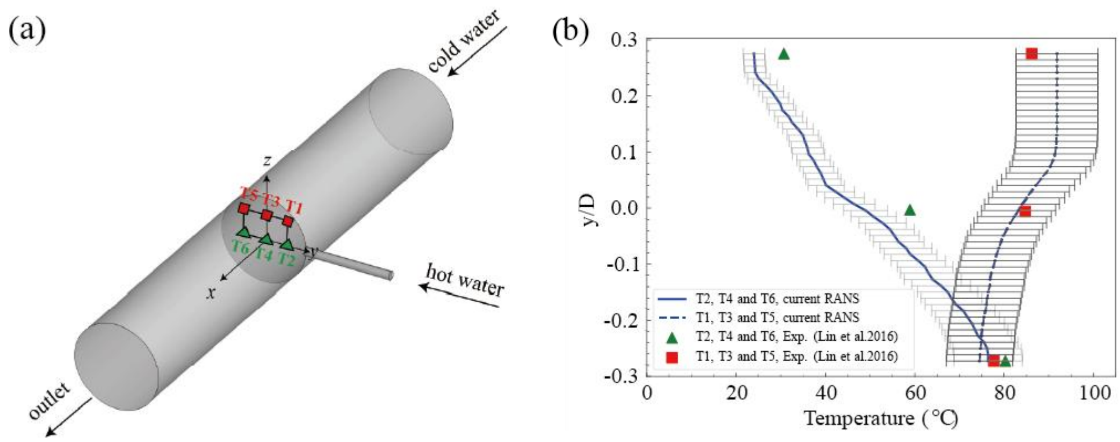


**Fig.5 Comparison of modelled fluid mixing with experimental data of Lin et al[29]. (a) Schematic diagram of the T-junction and mixing of cold and warm fluids; (b) comparison of the temperature profiles. The temperatures were measured along the monitoring points:**

**T1-T3-T5 (red squares) and T2-T4-T6 (green triangles). D denotes the diameter of the main pipe**

While it is challenging to simulate the differences between calculated values and measurements, the evaluation of model performance is enhanced by incorporating additional statistical measures. The corresponding observed $O_i$ and predicted $P_i$ are provided, and the statistical performance is evaluated using established metrics (e.g. Cheng et al[30], Duan and Ngan[31]) in this study, which include normalized mean square error ( $NMSE$ ), correlation coefficient ( $R$ ), score deviation ( $FB$ ), factor 2 ( $FAC2$ ), and hit rate ( $q$ ), i.e. :

$$NMSE = \frac{\sum_{i=0}^{N-1}(O_i - P_i)^2}{\sum_{i=0}^{N-1}(O_i P_i)} \quad (12)$$

$$R = \frac{\sum_{i=0}^{N-1}\left[\left(O_i - \frac{1}{N}\sum_{i=0}^{N-1}O_i\right)\left(P_i - \frac{1}{N}\sum_{i=0}^{N-1}P_i\right)\right]}{\left[\left(O_i - \frac{1}{N}\sum_{i=0}^{N-1}O_i\right)^2\right]^{1/2}\left[\left(P_i - \frac{1}{N}\sum_{i=0}^{N-1}P_i\right)^2\right]^{1/2}} \quad (13)$$

$$FB = \frac{\sum_{i=0}^{N-1}O_i - \sum_{i=0}^{N-1}P_i}{\frac{1}{2}\left(\sum_{i=0}^{N-1}O_i + \sum_{i=0}^{N-1}P_i\right)} \quad (14)$$

$$FAC2 = \frac{1}{N}\sum_{i=0}^{N-1}x_i, \text{其中} X_i = \begin{cases} 1, for\, 0.5 \le P_i/O_i \le 2.0 \\ 0, otherwise \end{cases} \quad (15)$$

$$q = \frac{1}{N}\sum_{i=0}^{N-1}x_i, \text{其中} X_i = \begin{cases} 1, for \left|\frac{O_i - P_i}{O_i}\right| \le \Delta_r, or \left|O_i - P_i\right| \le \Delta_a \\ 0, otherwise \end{cases} \quad (16)$$

where $N$ represents the total number of predictions, $\Delta_r$ denotes the allowed relative deviation, and $\Delta_a$ represents the allowed absolute deviation, reflecting the model’s ability to reproduce measured data[32]. The specified values of $\Delta_r = 0.25$ and $\Delta_a = 0.05$ align with recommendations of Eichhorn[33] and Santiago et al[34].

**Tab.4 Statistical performance measures of the RANS model against the experimental measurements of Lin et al[29]**

| statistical indicators | $NMSE$ | $R$ | $FB$ | $FAC2$ | $q$ |
|---|---|---|---|---|---|

| | | | | | |
|---|---|---|---|---|---|
| value | 0.007 | 0.988 | 0.046 | 1 | 1 |

$NMSE$ , $R$ and $FB$ are standard. $FAC2$ represents the fraction of the predicted value within the factor range of the two observed values. The hit rate ( $q$ ) measures the probability of being detected. A perfect model would be $NMSE = FB = 0.0$ , $R = FAC2 = q = 1.0$ (Chang and Hanna[35]; Ebrahimi et al[33]). The comparison with the experimental measurements of Lin et al[29] is summarized in Tab.4, showing that the model performance of all statistical indicators is satisfactory.

## 3 Influence of particle diameter on dust removal efficiency under different rotation angles of angle steel tray

Tab.5 shows the data parameters for the shale particles in a single refinery. Through the measurement of particle data, it is found that the volume fraction of particles entering the scrubber is less than 10%. Therefore, the DPM model was adopted to simulate the particle phase flow in the scrubber[36], and the capture of particles was used to calculate the dust removal efficiency. The selection of this method is based on the study of Jiang et al[37]. In this study, the VOF-DPM model is also adopted, and in the model setting, the methodology and parameter setting in the previous study are strictly followed to ensure the consistency and reliability of the model. In addition, the simulation results are in agreement with the operation conditions of scrubber in real industrial applications, which further verifies the effectiveness of the model. The dust removal efficiency is defined as the ratio of the dust content at the exit and the dust content at the entrance, and the interaction between discrete phase and continuous phase is considered in the analysis process.

**Tab.5 Shale test data from a refinery**

| | Water content（mg/L） | Oil content（mg/L） | Ash content（mg/L） |
|---|---|---|---|
| Mountain UP test | 358.9 | 0.71 | 1.72 |
| Mountain down test | 2181 | 1.03 | 1.26 |

### 3.1 Flow field stability analysis

Fig.6 shows the flow characteristics on the marks of six horizontal cross sections at different vertical levels in the washing tower. labeled $Y_2$, $Y_1$, $Y_0$, $Y_{-1}$, $Y_{-2}$, and $Y_{-3}$. In order to eliminate dust and other impurities attached to the inner surface of the scrubber, the washing liquid $H_2O$ is first used for pre-cleaning. In addition, the pre-cleaning of $H_2O$ not only helps to improve the heat and mass transfer efficiency after $CH_4$ injection, but also helps to establish an appropriate humidity and temperature environment in the tower. Fig. 6 presents the flow characteristics observed at the markings of six horizontal cross - sections located at various vertical levels within the scrubber.

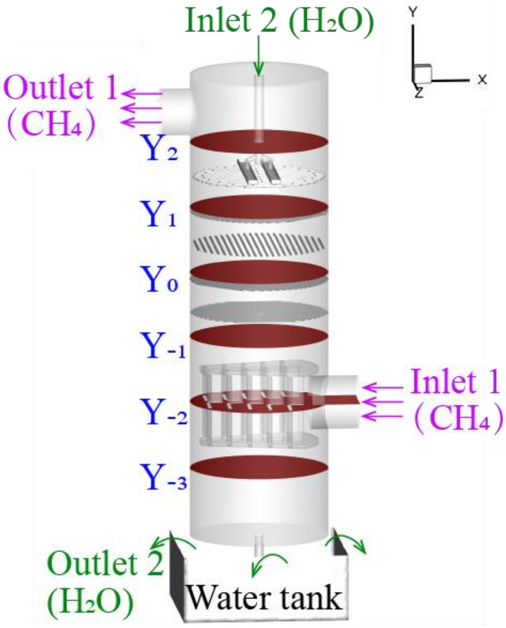


**Fig.6 Labelling of the horizontal cross sections at different vertical levels inside the scrubber.**

## 3.2 The influence of discrete relative continuous phase flow field

This study focuses on the effects of particle phase introduction on the pressure field and temperature field of the continuous phase, two parameters that are critical for understanding and predicting the hydrodynamic behavior and heat transfer efficiency in scrubbers.

Through the analysis of the pressure field, it is possible to evaluate the change of fluid flow resistance in the presence of particles, which is directly related to the flow field distribution and energy consumption in the scrubber.

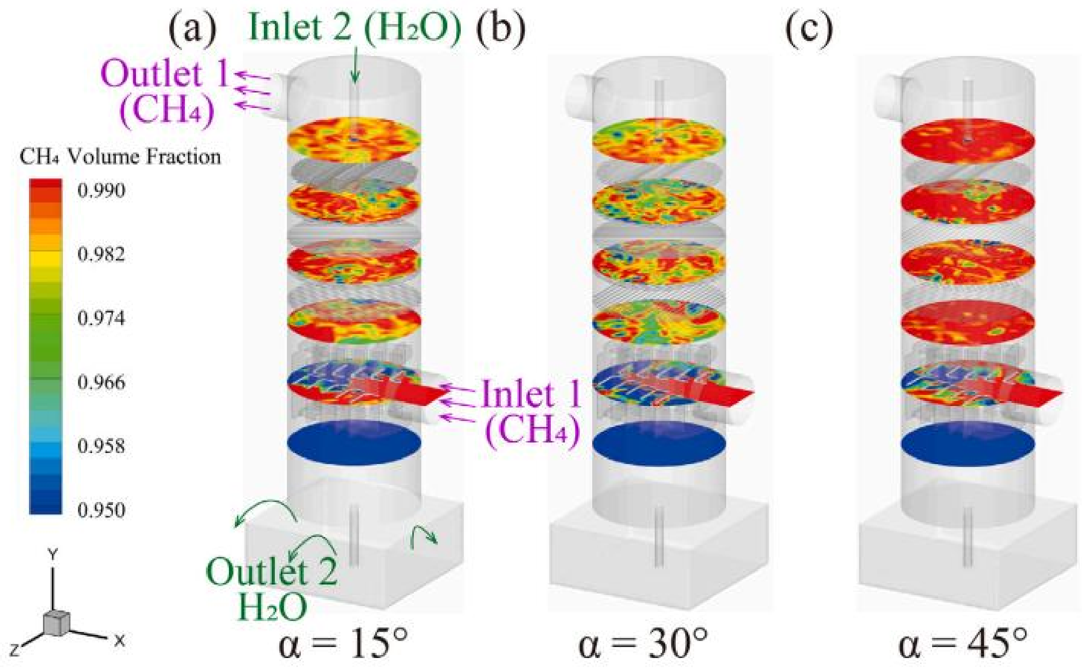


**Fig.7 $CH_4$ volume fraction in the different Y planes**

The increase of energy mainly comes from the addition of $CH_4$, so the distribution of $CH_4$ has a great influence on the particles in the washing tower, which can not only affect the heat transfer characteristics, but also change the flow of particles because of the high speed flow of $CH_4$. The $CH_4$ distribution is shown in Fig.7, and the overall distribution is relatively uniform with the increase of tower height. The monitoring of temperature field can evaluate the heat transfer characteristics of particles under the interaction of gas-liquid two phases, which has guiding significance for the realization of effective gas purification and temperature control. In addition, the modification of the turbulent characteristics of the particles relative to the continuous phase, including the change of the turbulent kinetic energy transfer and dissipation rate, is also considered in this study. Through this comprehensive analysis, we can understand the mechanism of particle phase in gas-liquid-solid three-phase system more comprehensively, and provide scientific basis for optimizing the design and operation of scrubber.

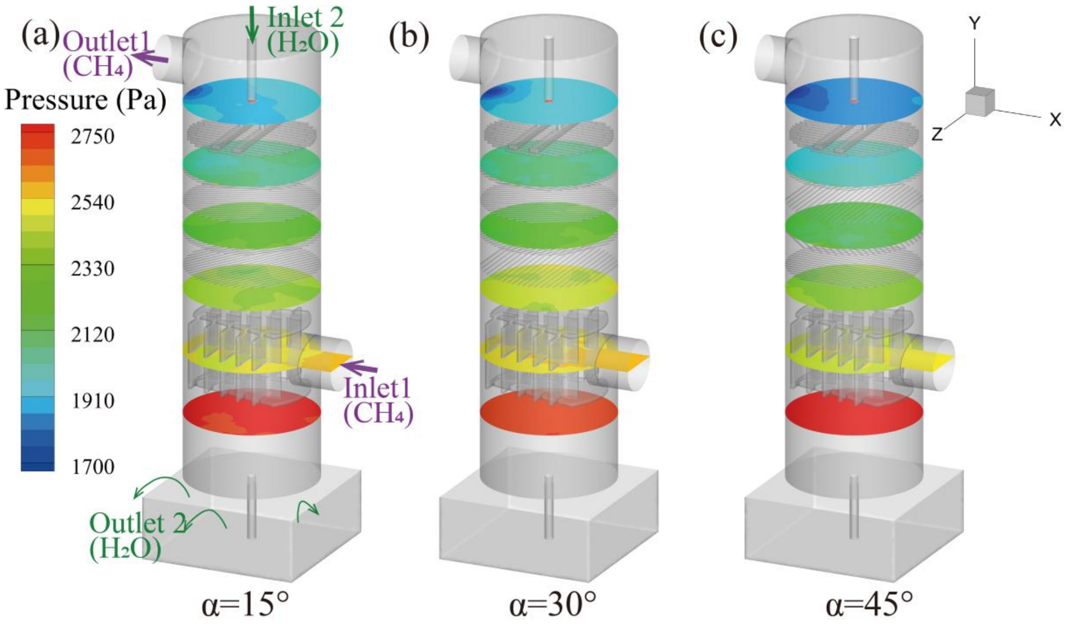


**Fig.8 Pressure field distribution after adding particles**

539

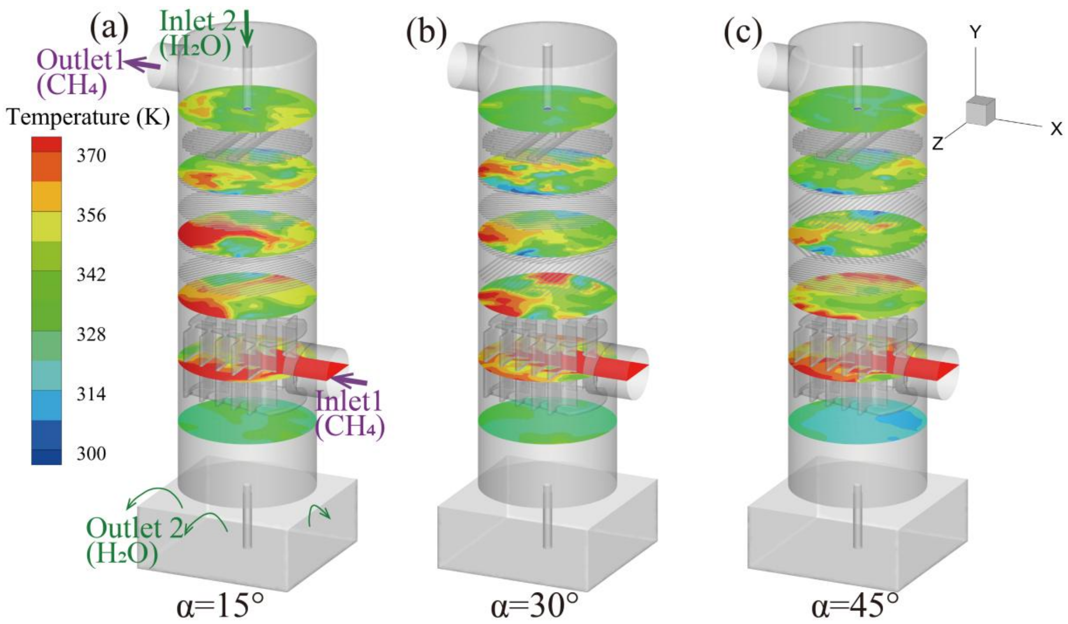


**Fig.9 Temperature field distribution after adding particles**

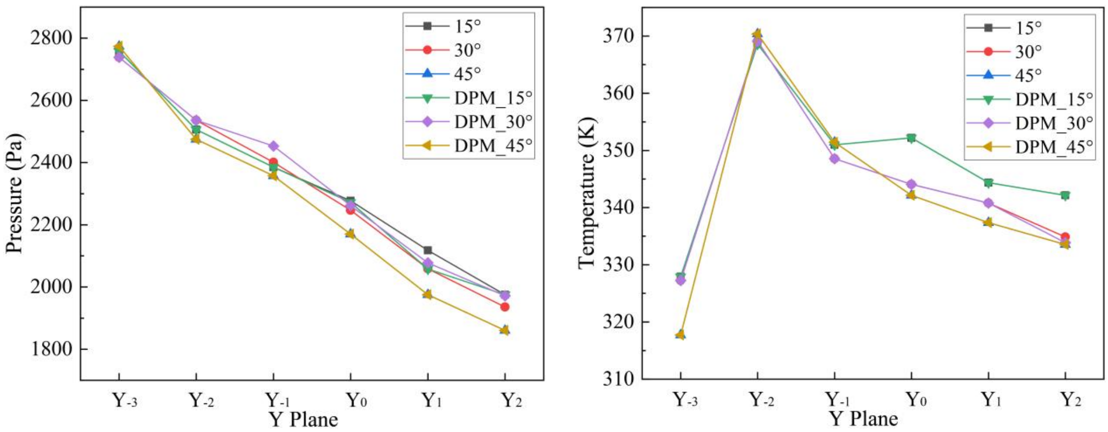


**Fig.10 Influence on pressure and temperature when particles are injected and not injected. The pressure and temperature curve data before injection of the pellet were obtained from the study by Zhao et al[18].**

Fig.8, Fig.9 and Fig.10 respectively show the distribution of temperature field and pressure field in the three-phase flow system after the introduction of particle phase, as well as the corresponding curves. Fig.8 shows the pressure field distribution after adding particles. It can be observed that the pressure distribution varies with different tray misalignment angles (α = 15°, 30°, and 45°). The overall pressure field appears to be relatively stable, with only slight differences in pressure magnitudes. This indicates that the addition of particles does not cause significant disruptions to the pressure field within the scrubber. The relatively small changes in pressure suggest that the current operating conditions are able to maintain a relatively smooth flow of the gas-liquid-solid mixture, which is beneficial for the stable operation of the scrubber. Moreover, the similar pressure patterns at different angles imply that the pressure is not highly sensitive to the tray misalignment within the range studied, at least in terms of the overall pressure distribution. However, further analysis is required to understand the potential subtle effects on local flow characteristics. The pressure and temperature of the three curves represented by 15°, 30° and 45° in Fig.10 are derived from L. Zhao et al[18]. 's research on the flow field inside the scrubber. These diagrams detail the effects of particles on the characteristics of continuous phase flow during the simulation. After the particle phase is added, the simulated pressure field and temperature field distribution do not change significantly, which means that the influence of particles relative to the overall flow field can be considered small under the current operating conditions, so the processing can be moderately simplified in the subsequent analysis.

This finding is of great significance for understanding and predicting the behavior of particles in gas-liquid-solid three-phase flow systems, and also provides valuable reference data for the design and optimization of scrubbers.

## 3.3 Discrete phase particle tracking

The number of particles analyzed in this study refers to the number of particle packets. The particle packet model is used to simulate the population of particles, which is based on both theoretical and practical considerations of the natural aggregation behavior of particles in turbulent flow. As the basic unit of analysis, the particle packet not only captures the dynamic of particle group economically and efficiently, but also maintains the characteristics of single particle, and realizes the effective approximation of complex multiphase flow. By controlling the total mass flow rate of the particle packet constant, the consistency with the actual working condition is ensured, and the influence of different tray arrangement on the particle capture efficiency is easily evaluated visually.

When the particles carried by gas enter the scrubber through the inlet, the particles of different sizes show different dynamic behavior and removal efficiency. Specifically, due to the relatively small inertial force, the movement trajectory of small particles is mainly controlled by gas flow mechanics, so it is limited by the internal structure of the scrubber (such as angle steel tray and trough liquid distributor) in the tower, and may eventually be taken out of the scrubber with gas, and cannot be effectively captured. In contrast, larger particles, due to their larger mass and inertia, are subjected to more significant forces such as gravity, drag and Saffman lift when moving in the air stream. The combined action of these forces makes it easier for large particles to be captured by the droplet after colliding with the falling wash droplet, and settle under the action of gravity, and finally deposit at the bottom of the wash tower, thus achieving effective removal of dust.

This process not only shows the complexity of gas-liquid-solid three-phase flow in scrubber, but also reveals the important role of tray structure in improving dust removal efficiency. By optimizing tray design and operating conditions, the dust removal performance of scrubber can be further improved, which has important guiding significance for gas purification technology in industrial applications.

In the particle result diagram made, Fig10a, b and c represent the scrubber at α=15°, α=30° and α=45°, respectively. The color of the trace represents different particle diameters, with the diameter of the particle ranging from 10 to 3000μm, with blue representing the smallest particle diameter and red representing the largest particle diameter. In the resulting graph when the number of particles captured is listed, the total number of particles injected, escaped, and captured represents the number of particle packages, because it is very expensive to track each particle in a particle flow system, so the particle packages with the same properties (diameter, velocity, and position) are characterized as one particle to form a particle package. The behavior of each particle pack is determined by the behavior of the particles inside; The number of particles in a particle packet can be either a decimal or a positive integer. Therefore, in the case of the same inlet particle flow, the number of particle packets is used to calculate the dust removal efficiency.

Fig.11 presents the particle trace diagrams when the average particle diameter is 100μm for different tray misalignment angles (α = 15°, 30°, and 45°).

For the α = 15° tray arrangement (Fig.11a), the particle tracks are relatively more dispersed. Some larger diameter particle tracks are visible at the bottom of the scrubber. The presence of these larger particles at the bottom could be due to the combined effect of gravity and the relatively less favorable interaction with the tray structure at this angle. The less organized particle movement may lead to a lower chance of effective capture. The fluid flow around the tray might not be optimized at this angle to direct the particles towards the liquid phase for capture. Additionally, the smaller angle may not provide sufficient opportunity for the particles to interact with the washing liquid droplets, resulting in a relatively lower dust removal efficiency as observed in the corresponding data.

When the tray is at α = 30° (Fig.11b), the particle distribution appears to be more concentrated in certain regions. The particles seem to follow a more directed path. This could be attributed to the enhanced interaction between the gas, liquid, and particles facilitated by the 30° tray misalignment. Under the influence of water's surface tension, particles may tend to aggregate together, increasing their effective mass and thus the gravitational force acting on them, which promotes their settling. Moreover, the more organized flow pattern at this angle allows the particles to have more frequent and effective collisions with the washing liquid droplets. The washing liquid, flowing in a more favorable manner due to the tray angle, can also exert a greater impact on the particles, causing them to be captured more efficiently. This is consistent with the relatively higher dust removal efficiency observed for this angle in the data.

For α = 45° (Fig.11c), the particle tracks show a distinct behavior. Some particles follow a more direct path towards the bottom, similar to the 30° case. The presence of larger diameter particles at the bottom is also evident, suggesting that gravity is playing a significant role. The differences in particle traces at this angle compared to the others may be related to the unique flow characteristics induced by the 45° tray misalignment. The larger angle may cause the particles to experience different fluid forces, such as stronger inertial forces and more complex flow patterns. While the overall behavior shows some similarities to the 30° case in terms of particle movement towards the bottom, the specific details of the flow may lead to a slightly different capture efficiency, as seen in the data.

These differences in particle traces at different tray angles are crucial as they directly impact the probability of particle capture. The more organized and directed the particle movement, the higher the likelihood of the particles coming into contact with the washing liquid and being trapped, thereby enhancing the dust removal efficiency.

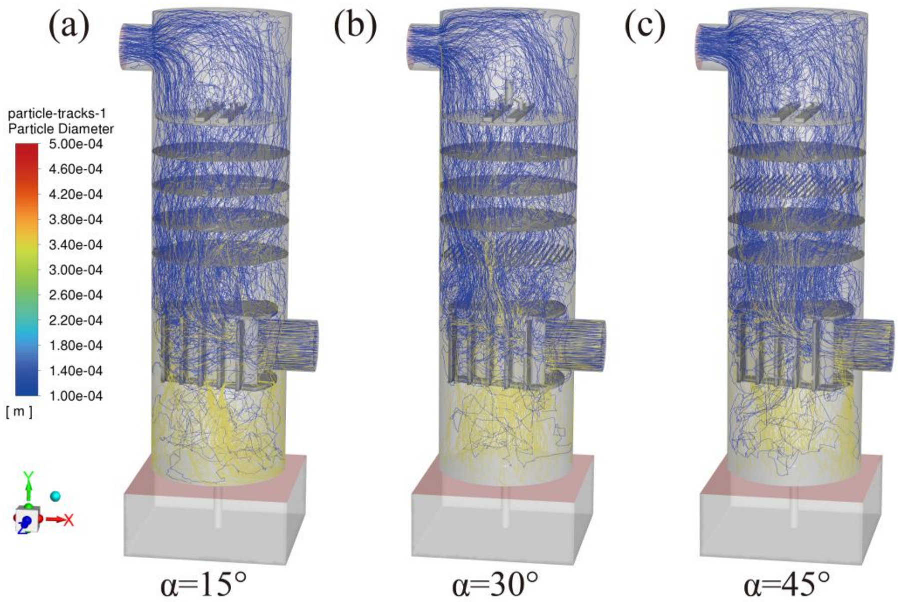


**Fig.11 Particle trace diagram when the average particle diameter is 100μm. (a) α=15°; (b) α=30°; (c) α=45°**

**Tab.6 Particle capture when the average particle diameter is 100μm**

| | Tracks | Escapes | Captures | Not tracked |
|---|---|---|---|---|
| α=15° | 554 | 173 | 381 | 0 |
| α=30° | 612 | 186 | 426 | 0 |
| α=45° | 652 | 198 | 453 | 1 |

Tab.6 shows the particle capture situation when the average particle diameter is 100μm for the three tray misalignment angles. When the angle steel tray is arranged at 15° and the particle flow is fixed, a total of 554 particles are injected. Out of these, 381 particles are captured, and 173 particles escape. The corresponding dust removal efficiency is calculated to be 68.8%. This relatively lower efficiency at 15° can be related to the particle trace observations in Fig.11a. The less efficient particle movement and interaction with the liquid phase, as discussed above, result in a lower capture rate.

When the tray arrangement angle is 30°, with a fixed injection particle flow rate, a total of 612 particles are injected, and 426 particles are captured, while 186 particles escape. The corresponding dust removal efficiency is 69.6%. The higher capture rate at 30° compared to 15° is consistent with the more favorable particle movement and interaction with the liquid phase as seen in Fig.11b. The enhanced flow pattern and particle-liquid interaction at this angle lead to a greater number of particles being trapped by the washing liquid.

For the 45° tray arrangement, a total of 652 particles are injected, 453 particles are captured, and 198 particles escape, resulting in a dust removal efficiency of 69.5%. Although the efficiency at 45° is slightly lower than at 30°, the particle capture data still show a significant number of particles being removed. The differences in capture rates between the three angles further emphasize the importance of tray misalignment in determining the dust removal efficiency. These data support our previous conclusion that the tray angle plays a crucial role in the dust removal process and that different angles can lead to varying levels of performance.

When the average diameter of the particles incident from the gas inlet is 200μm, the trace diagram of the particles is shown in Fig.12. By comparing the angle steel tray arranged at different angles, it can be seen that large particles accumulate at the bottom of the scrubber, and the number of large diameter particles is obviously more than α=15° when α=30° and α=45°. At α=45°, large particles accumulate and fall.

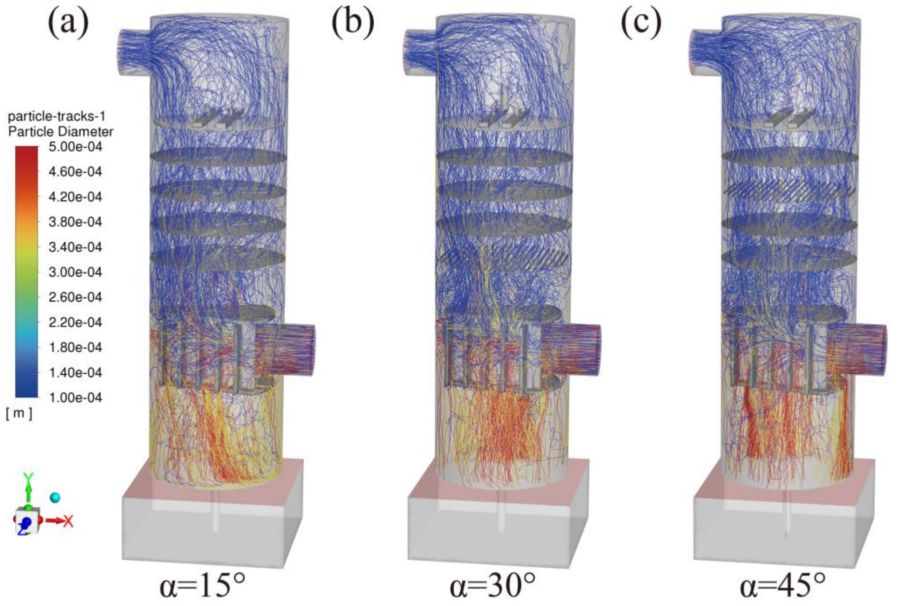


**Fig.12 Particle trace diagram when the average particle diameter is 200μm. (a) α=15° ; (b) α=30° ; (c) α=45°**

Tab.7 shows the particle capture situation when the average particle diameter is 200μm. When the angle steel tray is arranged at 15°, the particle flow rate is fixed. A total of 831 particles are injected, 655 particles are captured, and 173 particles escape. The corresponding dust removal efficiency is 78.8%. When the angle steel tray is arranged at 30°, a total of 918 particles are injected, 732 particles are captured, and 186 particles escape. The corresponding dust removal efficiency is 79.7%. When the angle steel tray is arranged at 45°, a total of 978 particles are injected, 775 particles are captured, and 198 particles escape. The corresponding dust removal efficiency is 79.2%.

**Tab.7 Particle capture when the average particle diameter is 200μm**

| | Tracks | Escapes | Captures | Not tracked |
|---|---|---|---|---|
| α=15° | 831 | 173 | 655 | 3 |
| α=30° | 918 | 186 | 732 | 0 |
| α=45° | 978 | 198 | 775 | 5 |

When the average diameter of the particles incident from the gas inlet is 300μm, the trace diagram of the particles and the particle capture data are shown in Fig.13 and Tab.8. By comparing the angle steel tray arranged at different angles, it can be seen that large particles accumulate at the bottom of the scrubber. In this case, the particle trajectory diagram and particle capture condition, that is, the dust removal efficiency, are the same as when the average diameter of the incident particle is 200μm.

In the actual simulation process, when the particle size is in the range of 200-300 μm, the particle motion characteristics and dust removal mechanism show similarities under the simulation conditions in this study. From the point of view of the force of particles, under the comprehensive influence of the main forces such as gravity and drag force, the motion trajectory of particles in this particle size range is similar to the interaction mode with the washing liquid. Under the setting of angle steel trays at different angles, the contact chance, collision probability and difficulty of being captured between the particles and the washing liquid are similar. As a result, under the same angle configuration of angle steel trays, the data such as the number of captured particles and the number of escaped particles are basically the same, and the dust removal efficiency is ultimately consistent.

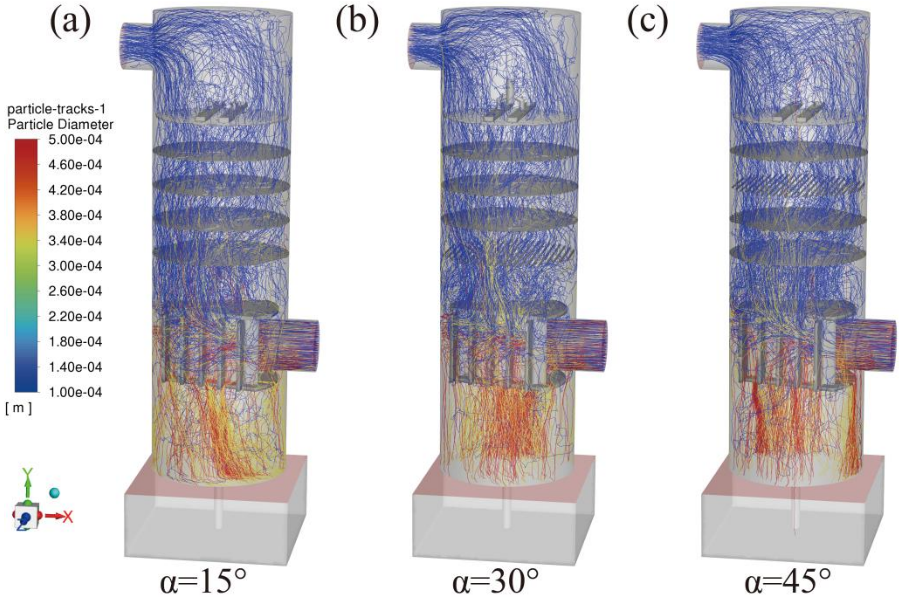


**Fig.13 Particle trace diagram when the average particle diameter is 300μm. (a) α=15°; (b) α=30°; (c) α=45°**

**Tab.8 Particle capture when the average particle diameter is 300μm**

| | Tracks | Escapes | Captures | Not tracked |
|---|---|---|---|---|
| α=15° | 831 | 173 | 655 | 3 |
| α=30° | 918 | 186 | 732 | 0 |
| α=45° | 978 | 198 | 775 | 5 |

When the average diameter of the particle incident from the gas inlet is 400μm, its movement trajectory in the scrubber can be clearly shown in Fig.14. Through the detailed comparative analysis of angle steel tray arranged at different angles, the internal relationship between the distribution of particulate matter in the tower and the dust removal efficiency can be revealed. This illustration shows that in the bottom area of the scrubber, there is a significant accumulation of larger particles, especially in the case of α=30° and α=45° angle steel tray configuration, the number of large diameter particles is significantly increased compared to the α=15° tray configuration. This phenomenon reveals the direct influence of different angle tray arrangement on the sedimentation and trapping effect of large particles.

The different angle settings of the angle steel tray play a decisive role in the movement trajectory, collision probability and contact chance of the particles carried by gas in the tower. When the tray angle increases (such as α=30° and α=45°), the particles are more likely to slide down the inclined plane under the action of gravity and washing liquid, and produce more frequent and more effective contact with the tray, thus increasing the possibility of large particles being trapped. Its large mass and inertia make it easier to overcome the drag force and settle to the bottom of the tower when it is in contact with the tray, thus forming an obvious aggregation phenomenon. On the contrary, the tray with a smaller rotation angle (such as α=15°) has a relatively weak interception effect on large particles, resulting in large particles more easily moving up with the air flow and failing to be effectively captured.

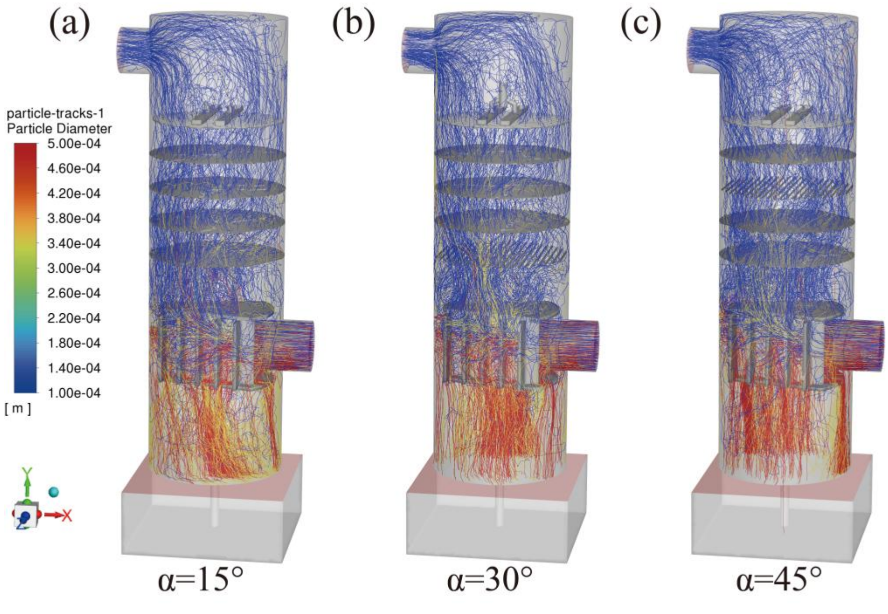


**Fig.14 Particle trace diagram when the average particle diameter is 400μm. (a) α=15°; (b) α=30°; (c) α=45°**

Tab.9 shows the particle capture situation when the average particle diameter is 400μm. When the angle steel tray is arranged at 15° and the particle flow rate is fixed, a total of 1108 particles are injected, 915 particles are captured, and 190 particles escape. The corresponding dust removal efficiency is 82.6%. When the angle steel tray is arranged at 30°, a total of 1224 particles are injected, 1015 particles are captured, and 209 particles escape. The corresponding dust removal efficiency is 83%. When the angle steel tray is arranged at 45°, a total of 1304 particles are injected, 1073 particles are captured, and 226 particles escape. The corresponding dust removal efficiency is 82.3%.

**Tab.9 Particle capture when the average particle diameter is 400μm**

| | Tracks | Escapes | Captures | Not tracked |
|---|---|---|---|---|
| α=15° | 1108 | 190 | 915 | 3 |
| α=30° | 1224 | 209 | 1015 | 0 |
| α=45° | 1304 | 226 | 1073 | 5 |

When the average diameter of the particles incident from the gas inlet is 500μm, the trace diagram of the particles is shown in Fig.15. By comparing the angle steel tray arranged at different angles, it can be seen that there is a large accumulation of large particles at the bottom of the scrubber, and the number of large diameter particles is obviously more than α=15° when α=30° and α=45°. At α=45°, a strip of aggregate falls, possibly because the particles hit the gas distributor and fall under the action of gravity.

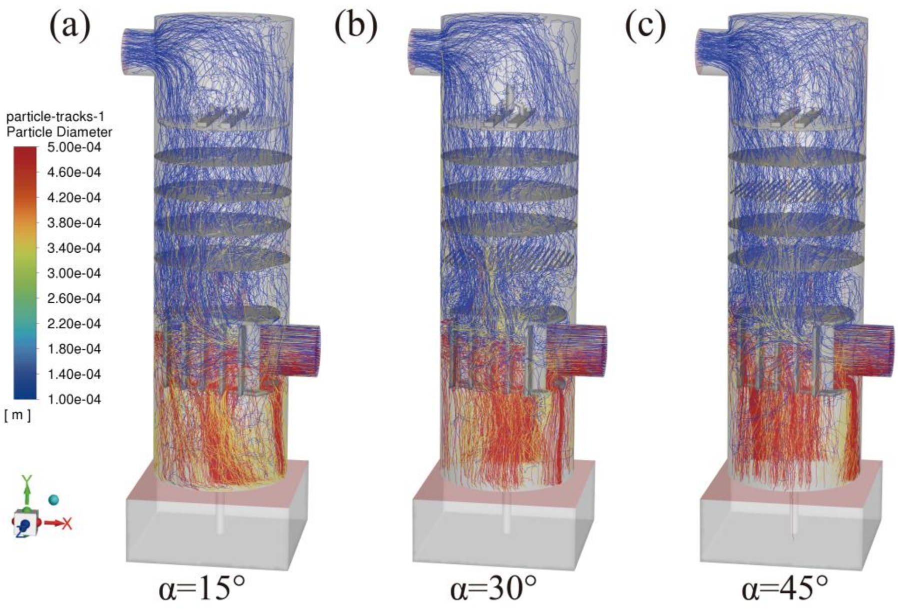


**Fig.15 Particle trace diagram when the average particle diameter is 500μm. (a) α=15°; (b)**

**α=30°; (c) α=45°**

Tab.10 shows the particle capture situation when the average particle diameter is 500μm. When the angle steel tray is arranged at 15° and the particle flow rate is fixed, a total of 1385 particles are injected, 1147 particles are captured and 233 particles escape. The corresponding dust removal efficiency is 82.8%. When the angle steel tray is arranged at 30°, the fixed injection particle flow rate, a total of 1530 particles are injected, 1274 particles are captured and 256 particles escape. The corresponding dust removal efficiency is 83.3%. When the angle steel tray is arranged at 45°, a total of 1630 particles are injected, 1340 particles are captured, and 285 particles escape. The corresponding dust removal efficiency is 82.2%.

**Tab.10 Particle capture when the average particle diameter is 500μm**

| | Tracks | Escapes | Captures | Not tracked |
|---|---|---|---|---|
| α=15° | 1385 | 233 | 1147 | 5 |
| α=30° | 1530 | 256 | 1274 | 0 |
| α=45° | 1630 | 285 | 1340 | 5 |

As can be seen from Fig.16, the overall trend shows that the dust removal efficiency increases with the increase of particle diameter, and the dust removal efficiency is the same when the particle diameter is 200μm and 300μm. This is because in this particle size range, the physical properties of the particles make them behave similarly in the scrubber, resulting in a stable dust removal efficiency. When the fixed particle diameter is analyzed which angle steel tray arrangement mode has higher dust removal efficiency, it is found that the dust removal efficiency is higher when α=30° before 350μm, and the dust removal efficiency is lowest when α=15°. The particle dust removal efficiency is high when α=30° is greater than 350μm, and the dust removal efficiency is lowest when α=45°.

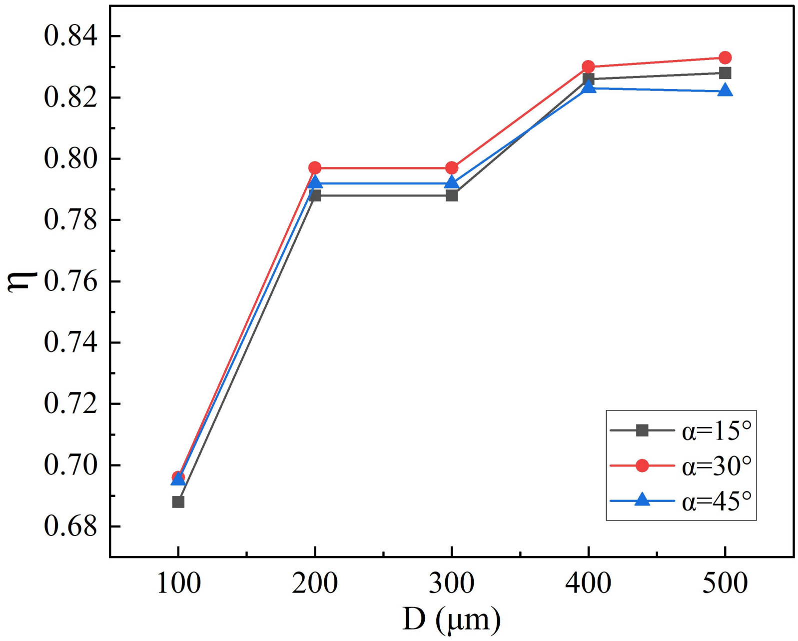


**Fig.16 Relationship between particle diameter and dust removal efficiency under different arrangement of tray layers**

When the particles and rising gas enter the scrubber together, the interaction between the air flow and the droplet not only affects the trajectory of the particles, but also determines their final departure and stay. Under the α=30° tray layout, the combined action of fluid tension and particle gravity is comprehensively analyzed, resulting in the improvement of sedimentation efficiency of larger particles, reflecting the direct result of the joint action of gas-liquid-solid three phases. At the tray dislocation angle of α=30°, the mixture of gas and washing liquid is enhanced. The uniform liquid and gas distribution helps the gas, liquid and particles to contact more fully, enhance the mass transfer effect, and thus improve the removal efficiency of particles; The α=30° tray dislocation angle performs well in reducing the pressure of the purified gas, which helps the gas discharge and reduces the impact of the outlet gas on the discharge line. The lower pressure drop means that the gas flows more smoothly in the tower, which is conducive to the movement and settlement of particles in the tower, further improving the efficiency of dust removal.

## 3.4 Practical implications of particle tracking results

The detailed particle tracking results obtained in this study have significant implications for industrial scrubber designs. By understanding the behavior of particles of different sizes within the scrubber under various tray configurations, we can make informed decisions to optimize the scrubber's performance.

For particles with diameters below 200μm, their movement is mainly influenced by gas flow mechanics. This indicates that in industrial scrubber designs, special attention should be paid to enhancing the initial contact between the gas and the liquid phase. For example, the design of the gas inlet and the initial distribution of the washing liquid can be optimized to increase the probability of small particles being captured at the early stage. This could involve using more efficient gas distributors or liquid spraying systems that can create finer droplets and a more uniform distribution, thereby improving the capture rate of small particles.

When the particle diameter is between 200μm and 350μm, we observed that the tray with a misalignment angle of $\alpha = 30°$ shows better dust removal efficiency. In industrial applications, this suggests that for scrubbers dealing with particles in this size range, setting the tray angle to 30° can enhance the sedimentation and trapping of particles. This can be achieved by adjusting the manufacturing and installation process of the trays to ensure the accurate alignment at this angle. Additionally, the design of the tray structure can be further optimized to take full advantage of the enhanced gas-liquid-solid interaction at this angle, such as modifying the shape or surface texture of the trays to promote better particle capture.

For particles larger than 350μm, the $\alpha = 30°$ tray configuration also performs well in terms of dust removal efficiency. In industrial scrubber designs, this implies that for processes that generate a significant amount of large particles, maintaining the tray at this angle can ensure effective removal. Moreover, the study also shows that at this angle, the pressure drop of the purified gas is relatively low, which is beneficial for the smooth operation of the scrubber. This means that the overall energy consumption of the scrubber can be reduced, as a lower pressure drop requires less energy for gas to flow through the system. Therefore, in industrial applications, not only can the dust removal performance be improved, but also the operational cost can be optimized by adopting the appropriate tray angle based on the particle size distribution.

In summary, the particle tracking results provide valuable insights that can directly guide the design and operation of industrial scrubbers, enabling engineers to make more efficient and effective choices to meet the specific requirements of different industrial processes.

# 4 Conclusion

In this study, we have investigated the impact of the inner angle steel tray misalignment and particle diameter on the dust removal efficiency in a scrubber tower. Through a combination of experimental and simulation methods, several key findings have emerged.

We established the geometric model of the scrubber based on the actual equipment in a refinery and employed CFD with the VOF and DPM to solve the relevant equations. After grid independence verification and model validation, we found that the dust removal efficiency generally increases with the increase of particle diameter. Specifically, when the particle diameter is in the range of 200 – 300 μm, the efficiency remains consistent. Before 350μm, the highest efficiency is achieved at a tray misalignment angle of $\alpha = 30°$, and the lowest at $\alpha = 15°$; above 350μm, the highest efficiency is still at $\alpha = 30°$, while the lowest is at $\alpha = 45°$. The tray angle also affects the air distribution uniformity within the scrubber. It was observed that at $\alpha = 45°$, the size and distribution of the perforation are more uniform, which contributes to a more uniform flow channel, thereby enhancing the uniformity of gas-liquid mixing. This uniformity not only improves the heat and mass transfer efficiency of the scrubber but also boosts the dust removal efficiency, particularly when dealing with larger particles.

The practical implications of these findings are significant for industrial scrubber designs. For example, in industrial applications, when dealing with particles in the size range where $\alpha = 30°$ shows better performance (below 350μm), adjusting the tray angle to 30° can enhance sedimentation and trapping of particles. This can be realized by precisely controlling the manufacturing and installation process to ensure accurate alignment. For processes generating a large amount of large particles (above 350μm), maintaining the tray at 30° can ensure effective removal and reduce the pressure drop of the purified gas, optimizing energy consumption.

Future studies could further explore other tray configurations. This could involve varying the number of tray layers, the shape and size of the angle steel, or the pattern of misalignment to potentially identify even more optimal configurations for higher dust removal efficiencies. Secondly, investigating the behavior of different particle materials within the scrubber is essential. Understanding how the physical and chemical properties of particles, such as surface charge, hydrophobicity, and reactivity, influence their interaction with the gas and liquid phases and the tray structure could lead to more customized scrubber designs for specific industrial applications.

In conclusion, this research provides a scientific basis for optimizing scrubber design and operation. It systematically explores the influence of tray angle and particle diameter on dust removal efficiency, filling a research gap in this area and offering practical guidance for the improvement of scrubber technology in industrial applications. The proposed future research directions offer opportunities for further advancements in this field.

# Declarations

**Author contributions:** Hai Xin and Yong Yang were responsible for the study design and experiment execution and co-authored the main text of the paper. Yulin Yan is responsible for data analysis and chart production, especially the preparation of figures 1 to 4. Zhenyu Xu provided critical theoretical support and experimental guidance. Xianyu Feng participated in the experimental design and data analysis, and proofread the paper.

**Competing interests policy:** the authors declare no competing interest.

**Consent to Publish declaration:** this article is a PNAS Direct Submission. Published under the PNAS license.

**Data Availability:** all data is included in the manuscript.

**Dual publication:** the results/data/figures in this manuscript have not been published elsewhere, nor are they under consideration by another publisher.

**Funding Declaration:** this work was supported by the PhD Start-up Fund (Grant No. 1100130252).

**Third party material:** all of the material is owned by the authors.

**Ethics Declaration:** Ethics approval is not applicable to this study as it did not involve human or animal subjects.

**Consent to Participate Declaration:** Consent to participate is not applicable as the study utilized publicly available data.

## References


[1] YANG, Y, SU, Q, ZHENG, C, et al. Emission characteristics of filterable particulate matter and condensable particulate matter from coal-fired power plants, Case Studies in Thermal Engineering[J]. 2022, 35: 102145. https://doi.org/10.1016/j.csite.2022.102145.

[2] ZHOU, Y, ZHU, R, WEI, G. Recent advancements in source reduction and recycling technologies for converter dust, Energy Reports[J]. 2022, 8: 7274-7285. https://doi.org/10.1016/j.egyr.2022.05.234.

[3] TANG, W, WU, C-W, LIN, S-L, et al. Enhanced mitigation of inhalable particles and fine particle-bound pahs from a novel hazardous waste-power plant candidate, Environ. Pollut.[J]. 2023, 343: 15. https://doi.org/10.1016/j.envpol.2023.123220.

[4] JIANGYUAN, Q, NANA, Q, KAI, Z. Cfd modeling for $no_x$ absorption accompanying with $so_2$ in wet flue gas desulfurization scrubber based on gas-phase ozone oxidation, Process Saf. Environ. Prot.[J]. 2022, 159: 685-697. https://doi.org/10.1016/j.psep.2022.01.037.

[5] TURPIN, A, COUVERT, A, LAPLANCHE, A, PAILLIER, A. Mass transfer and deodorization efficiency in a countercurrent spray tower for low superficial gas velocities, Can. J. Chem. Eng.[J]. 2009, 87(1): 53-59. https://doi.org/10.1002/cjce.20084.

[6] LI, S, LIAO, Y. Cfd investigation of bubble breakup and coalescence in a rectangular pool-scrubbing column, Nucl. Eng. Des.[J]. 2024, 425: 113342. https://doi.org/10.1016/j.nucengdes.2024.113342.

[7] PAN, D, WU, H, YANG, L. Investigation of the relationship between droplet and fine particle emissions during the limestone–gypsum wet flue gas desulfurization process, Energy Fuels[J]. 2017, 31(6): 6472–6477. https://doi.org/10.1021/acs.energyfuels.7b00423.

[8] XINLI, Z, JIFENG, J, XIAOCHUAN, L, et al. Potential use of wet scrubbers for the removal of tobacco dust particles in the tobacco industry, Atmosphere[J]. 2022, 13(3): 380. https://doi.org/10.3390/atmos13030380.

[9] XU, Y, LIU, X, QI, J, et al. Evolution of particulate matter in a municipal solid waste incinerator: Probing into the effects of a rotary spray semi-dry scrubber and a baghouse, Energy Fuels[J]. 2021, 35: 4237-4245. https://doi.org/10.1021/acs.energyfuels.0c04144.

[10] ZHU, Y, WAN, Q, HOU, Q, et al. Analysis of diffusion characteristics and influencing factors of particulate matter in ship exhaust plume in arctic environment based on cfd, Atmosphere[J]. 2024, 15(5): 580. https://doi.org/10.3390/atmos15050580.

[11] WEI, T, LI, X, WANG, D, LIU, Y. Multiscale dynamic distribution characteristics of dust collectors in wet scrubber based on image fields, J. Air Waste Manage. Assoc.[J]. 2020, 70(9): 847-861. https://doi.org/10.1080/10962247.2020.1778136.

[12] COPELAND, C R, KAWATRA, S K. Design of a dust tower for suppression of airborne particulates for iron making, Miner. Eng.[J]. 2011, 24: 1459-1466. https://doi.org/10.1016/j.mineng.2011.07.008.

[13] KIM, H-G, KIM, H-J, LEE, M-H, KIM, J-H. Experimental study on the enhancement of particle removal efficiency in spray tower scrubber using electrospray, Asian Journal of Atmospheric Environment[J]. 2014, 8: 89-95. https://doi.org/10.5572/ajae.2014.8.2.089.

[14] BACHER, C, RIEBEL, U. Electrohydrodynamically enhanced mass transfer in a wetted-wall column, Chem. Eng. Res. Des.[J]. 2021, 167: 183-197. https://doi.org/10.1016/j.cherd.2021.01.006.

[15] SEN, N, SINGH, K K, PATWARDHAN, A W, et al. Cfd-pb studies on effect of internals on specific interfacial area in a pulsed sieve plate columns, Chem. Eng. Res. Des.[J]. 2023, 202: 235-247. https://doi.org/10.1016/j.cherd.2023.12.003.

[16] BANDYOPADHYAY, A. Abatement of particulate-laden so2 in tapered bubble column with internals, Air Quality, Atmosphere & Health[J]. 2009, 2: 147-155. https://doi.org/10.1007/s11869-009-0041-3.

[17] HUA, J, ZHANG, X-B, LI, H, LUO, Z-H. Experiment and simulation study on the effect of internals in gas–liquid bubble columns with a low aspect ratio, Ind. Eng. Chem. Res.[J]. 2024, 63: 4595-4604. https://doi.org/10.1021/acs.iecr.3c04180.

[18] ZHAO, L, FENG, X, CHEN, J, et al. Gas purification in a scrubber tower: Effects of the multilayer tray misalignment, Case Studies in Thermal Engineering[J]. 2024, 55: 104130. https://doi.org/10.1016/j.csite.2024.104130.

[19] TSENG, C-C, LI, C-J. Numerical investigation of the inertial loss coefficient and the porous media model for the flow through the perforated sieve tray, Chem. Eng. Res. Des.[J]. 2015https://doi.org/10.1016/j.cherd.2015.12.017.

[20] ABBASNIA, S, NASRI, Z, NAJAFI, M. Comparison of the mass transfer and efficiency of nye tray and sieve tray by computational fluid dynamics, Sep. Purif. Technol.[J]. 2019, 215: 276-286. https://doi.org/10.1016/j.seppur.2019.01.010.

[21] LAVASANI, M S, RAHIMI, R, ZIVDAR, M. Hydrodynamic study of different configurations of sieve trays for a dividing wall column by using experimental and cfd methods, CHEM ENG PROCESS[J]. 2018, 129: 162-170. https://doi.org/10.1016/j.cep.2018.05.008.

[22] ZHAO, H, LI, L, JIN, J, LI, Q. Cfd simulation of sieve-fixed valve tray hydrodynamics, Chem. Eng. Res. Des.[J]. 2017, 129: 55-63. https://doi.org/10.1016/j.cherd.2017.10.034.

[23] SALINS, S S, KUMAR, S, CHOUHAN, J, et al. Experimental performance of a spray tower system for water desalination and indoor thermal comfort, Process Saf. Environ. Prot.[J]. 2023, 180: 122-135. https://doi.org/10.1016/j.psep.2023.10.007.

[24] CHEN, S, ZHAO, X, XIAO, Z, et al. Enhancement of fine particle removal through flue gas cooling in a spray tower with packing materials, J. Hazard. Mater.[J]. 2024, 478: 135390. https://doi.org/10.1016/j.jhazmat.2024.135390.

[25] MAKKINEJAD, N. Temperature profile in countercurrent/cocurrent spray towers, Int. J. Heat Mass Transfer[J]. 2001, 44(2): 429-442. https://doi.org/10.1016/s0017-9310(00)00088-0.

[26] WANG, C, LIU, M, LIU, H, et al. Numerical analysis of co2 absorption characteristics in industrial flue gas mineralization spray tower reactor, Sep. Purif. Technol.[J]. 2024, 354: 129051. https://doi.org/10.1016/j.seppur.2024.129051.

[27] SUN, Y, JIANG, J, LI, J, et al. Simulation of gas-liquid-solid three-phase flow process and particle removal characteristics in liquid chamber of scrubbing tower, J. Eng. Thermophys.[J]. 2020, 29: 477-491. https://doi.org/10.1134/s1810232820030121.

[28] KALITZIN, G, MEDIC, G, IACCARINO, G, DURBIN, P. Near-wall behavior of rans turbulence models and implications for wall functions, J. Comput. Phys.[J]. 2005, 204(1): 265-291. https://doi.org/10.1016/j.jcp.2004.10.018.

[29] LIN, C H, CHEN, M S, FERNG, Y M. Investigating thermal mixing and reverse flow characteristics in a t-junction by way of experiments, Appl. Therm. Eng.[J]. 2016, 99: 1171-1182. https://doi.org/10.1016/j.applthermaleng.2016.02.009.

[30] CHENG, L, XIA, G. Fundamental issues, mechanisms and models of flow boiling heat transfer in microscale channels, Int. J. Heat Mass Transfer[J]. 2017, 108: 97-127. https://doi.org/10.1016/j.ijheatmasstransfer.2016.12.003.

[31] DUAN, G, NGAN, K. Effects of time-dependent inflow perturbations on turbulent flow in a street canyon, Boundary-Layer Meteorology[J]. 2017, 167: 257-284. https://doi.org/10.1007/s10546-017-0327-1.

[32] FRANKE, J, STURM, M, KALMBACH, C. Validation of openfoam 1.6.X with the german vdi guideline for obstacle resolving micro-scale models, Journal of Wind Engineering and Industrial Aerodynamics[J]. 2012, 104-106: 350-359. https://doi.org/10.1016/j.jweia.2012.02.021.

[33] EBRAHIMI, M, CRAPPER, M. Cfd–dem simulation of turbulence modulation in horizontal pneumatic conveying, Particuology[J]. 2017, 31: 15-24. https://doi.org/10.1016/j.partic.2016.05.012.

[34] SANTIAGO, J L, MARTILLI, A, MARTíN, F. Cfd simulation of airflow over a regular array of cubes. Part i: Three-dimensional simulation of the flow and validation with wind-tunnel measurements, Boundary-Layer Meteorology[J]. 2006, 122: 609-634. https://doi.org/10.1007/s10546-006-9123-z.

[35] CHANG, J C, HANNA, S R. Air quality model performance evaluation, Meteorology and Atmospheric Physics[J]. 2004, 87: 167-196. https://doi.org/10.1007/s00703-003-0070-7.

[36] MASSOUDI FARID, M, JEONG, H J, KIM, K H, et al. Numerical investigation of particle transport hydrodynamics and coal combustion in an industrial-scale circulating fluidized bed combustor: Effects of coal feeder positions and coal feeding rates, Fuel[J]. 2017, 192: 187-200. https://doi.org/10.1016/j.fuel.2016.12.025.

[37] JIANG, B, HE, D, ZHANG, L, et al. Vof-dpm simulations of gas-liquid-solid scrubbing chambers with two gas intake modes, J. Eng. Thermophys.[J]. 2019, 28: 345–358. https://doi.org/10.1134/s1810232819030056.